Beyond the Born–Oppenheimer approximation: High-resolution overtone spectroscopy of H 2 D + and D 2 H +

Michal Fárník, Scott Davis, Maxim A. Kostin, Oleg L. Polyansky, Jonathan Tennyson, and David J. Nesbitt

Citation: The Journal of Chemical Physics **116**, 6146 (2002); doi: 10.1063/1.1458244
View online: http://dx.doi.org/10.1063/1.1458244
View Table of Contents: http://scitation.aip.org/content/aip/journal/jcp/116/14?ver=pdfcov
Published by the AIP Publishing

Beyond the Born–Oppenheimer approximation: High-resolution overtone spectroscopy of H_2D^+ and D_2H^+

Michal Fárník and Scott Davis
JILA, University of Colorado and National Institute of Standards and Technology, and Department of Chemistry and Biochemistry, University of Colorado, Boulder, Colorado 80309-0440

Maxim A. Kostin,[a] Oleg L. Polyansky,[a] and Jonathan Tennyson
Department of Physics and Astronomy, University College London, London WC1E 6BT, United Kingdom

David J. Nesbitt
JILA, University of Colorado and National Institute of Standards and Technology, and Department of Chemistry and Biochemistry, University of Colorado, Boulder, Colorado 80309-0440

(Received 6 November 2001; accepted 17 January 2002)

Transitions to overtone $2\nu_2$ and $2\nu_3$, and combination $\nu_2+\nu_3$ vibrations in jet-cooled H_2D^+ and D_2H^+ molecular ions have been measured for the first time by high-resolution IR spectroscopy. The source of these ions is a pulsed slit jet supersonic discharge, which allows for efficient generation, rotational cooling, and high frequency (100 KHz) concentration modulation for detection via sensitive lock-in detection methods. Isotopic substitution and high-resolution overtone spectroscopy in this fundamental molecular ion permit a systematic, first principles investigation of Born–Oppenheimer ''breakdown'' effects due to large amplitude vibrational motion as well as provide rigorous tests of approximate theoretical methods beyond the Born–Oppenheimer level. The observed overtone transitions are in remarkably good agreement (<0.1 cm^{-1}) with non-Born–Oppenheimer *ab initio* theoretical predictions, with small but systematic deviations for $2\nu_2$, $\nu_2+\nu_3$, and $2\nu_3$ excited states indicating directions for further improvement in such treatments. Spectroscopic assignment and analysis of the isotopomeric transitions reveals strong Coriolis mixing between near resonant $2\nu_3$ and $\nu_2+\nu_3$ vibrations in D_2H^+. Population-independent line intensity ratios for transitions from common lower states indicate excellent overall agreement with theoretical predictions for D_2H^+, but with statistically significant discrepancies noted for H_2D^+. Finally, H_2D^+ versus D_2H^+ isotopomer populations are analyzed as a function of D_2/H_2 mixing ratio and can be well described by steady state kinetics in the slit discharge expansion. © *2002 American Institute of Physics.* [DOI: 10.1063/1.1458244]

I. INTRODUCTION

Protonated molecular hydrogen, H_3^+, is arguably the most fundamental molecular ion, playing a central role in a wide range of chemistry, physics, and astronomy.[1] At the theoretical level, this simplest of polyatomic molecules (i.e., three H nuclei and two electrons) has served as a benchmark system for development of high accuracy *ab initio* methods, especially as a prototype of treatment of $2e^-$ three-center bonding. In addition to its fundamental theoretical challenges, the H_3^+ ion is also of significant experimental relevance, since it is readily formed via ion–molecule reaction of molecular hydrogen with H_2^+,

$$H_2^+ + H_2 \rightarrow H_3^+ + H. \tag{1}$$

As a result, H_3^+ plays a key role in environments where molecular hydrogen gas is ionized, specifically in molecular hydrogen dominated plasmas. Since hydrogen is by far the most abundant element in the universe, with molecular hydrogen dominating in the cool regions, formation of H_3^+ ions is therefore expected to be of ubiquitous astrophysical significance. Indeed, H_3^+ has already been detected in the atmospheres of planets[2–4] and discovered both in molecular clouds[5–7] as well as the diffuse interstellar medium.[8,9]

As a consequence of such broad scientific interest, the H_3^+ ion and its isotopomers have represented ongoing targets of extensive experimental and theoretical effort.[10–15] The laboratory spectrum of H_3^+ ion was first measured in 1980 by Oka,[16] followed by spectroscopic studies of fundamental,[17,18] overtone,[19,20] and vibrational hot bands.[21] It is worth noting that even partially deuterated isotopomers of H_3^+ can also be of astrophysical importance, despite the fact that the cosmic abundance of deuterium is generally accepted to be only $\approx 10^{-5}$ of that of hydrogen. This is because exothermicities of H/D exchange reactions are driven by zero-point vibrational effects, which therefore strongly favor D versus H atom incorporation. Particularly in cold interstellar regions, this can lead to greatly enhanced isotopic fractionation effects which has led to recent detection[22] of ortho H_2D^+ via telescopes operating in the submillimeter region. This has in turn stimulated laboratory interest in these partially deuterated molecule ions. For example, the fundamental vibrational bands have also been observed and analyzed for both H_2D^+ ions[23,24] and D_2H^+ ions.[25,26] Due to lower

[a]Permanent address: Institute of Applied Physics, Russian Academy of Science, Nizhny Novgorod, Russia.

populations and weak transition strengths, however, it has proven challenging to extend such isotopomer studies into the overtone region, despite the need for such efforts to guide astronomical observations. As the primary thrust of this work, overtone/combination band transitions for these partially deuterated isotopomers are reported for the first time, using the high-resolution IR spectroscopy combined with concentration modulated slit discharge techniques to achieve the requisite sensitivity levels.

In addition to astrophysical importance, there are other compelling reasons for fundamental spectroscopic interest in these isotopomers. Though a reasonably accurate description of two-electron bonding in H_3^+ and isotopomers is available from conventional electronic structure calculations, the level of effort required to match experimental observation to spectroscopic accuracy is far from trivial. Specifically, large amplitude motion of the H/D nuclei leads to considerable complications and challenges in the nuclear dynamics for this light three-atom system. Indeed, Tennyson and co-workers[27,28] have clearly shown that a large contribution to error in the *ab initio* determination of H_3^+ rotation–vibration state energies arises from the breakdown of the fundamental Born–Oppenheimer approximation, i.e., sufficiently rapid electronic motion on the time scale of nuclear displacements to justify the concept of a potential energy surface (PES). In fact, the magnitude of such effects for H_3^+ and isotopomers is on the order of several cm^{-1} even for fundamental vibration/rotation levels; this is already 10^3-fold in excess of high-resolution Doppler limited spectroscopic uncertainties and predicted to increase further with overtone excitation. The existence of such non-Born–Oppenheimer effects undermines the simple yet virtually universal picture of nuclear dynamics occurring on a well defined, isotopically invariant potential surface. Detailed overtone studies of asymmetrically substituted isotopomers such as H_2D^+ and D_2H^+ are likely to prove especially enlightening, since these ions require additional non-Born–Oppenheimer corrections[29] that are absent in the more symmetric H_3^+ and D_3^+.

Exact rovibrational solution of H_3^+ and isotopomers as a full five-particle system remains an unsolved challenge. Nevertheless, progress in these directions has been extremely promising based on approximate three particle variational calculations with suitably modified potentials and effective non-Born–Oppenheimer kinetic energy terms in the Hamiltonian.[30] A twin track approach has been adopted, with initial studies improving *ab initio* estimates of both the Born–Oppenheimer potential and the adiabatic correction using previously observed spectroscopic data and more recent studies modeling these using an entirely *ab initio* procedure.[30] Indeed, predictions based on this *ab initio* procedure now reproduce existing experimental data for H_3^+ to nearly spectroscopic levels of precision,[30] i.e., within a few hundredths of a cm^{-1}. By virtue of the additional non-Born–Oppenheimer terms in the Hamiltonian, a particularly stringent test is provided by the asymmetrically substituted isotopomers, which to date have not been observed beyond the fundamental manifold.

This motivates the current high-resolution overtone studies of the H_2D^+ and D_2H^+ species, which form the central thrust of this paper. Our approach can be simply stated. To successfully obtain these spectra, slit jet discharge methods have been modified to ''synthesize'' high densities of partially deuterated molecular ions, in a jet-cooled configuration suitable for direct absorption IR laser spectroscopy at the shot noise limit. State-of-the-art non-Born–Oppenheimer theoretical predictions are then used to expedite high-resolution searches for overtone stretching/bending rovibrational $2\nu_2$, $2\nu_3$, and $\nu_2+\nu_3$ transitions in both H_2D^+ and D_2H^+. Measured line positions and intensities are then compared with theoretical predictions, permitting a rigorous evaluation of such non-Born–Oppenheimer models at high internal energies and as a systematic function of isotopomeric composition.

The organization of this paper is as follows. Section II presents a brief description of the experimental apparatus, with particular emphasis on the slit discharge source and recently implemented concentration modulation technique for study of jet-cooled ions. The spectroscopic results are presented in Sec. III, followed by detailed comparison with theoretical predictions from non-Born–Oppenheimer model calculations. Section IV presents a spectroscopic assignment highlighting the significant role of Coriolis interaction, followed in Sec. V by analysis of line intensities and ion state populations. Section VI presents a steady state kinetic model that successfully accounts for observed H_2D^+ versus D_2H^+ ion concentrations as a function of H_2/D_2 mixing ratio, which when coupled with nuclear spin conservation rules, provides a preliminary basis for interpretation of ortho versus para populations. Section VII summarizes and concludes the paper.

II. EXPERIMENT

The present studies have been performed with the near-IR high-resolution spectrometer and a pulsed, slit supersonic discharge source,[31,32] for which the concentration modulation technique has been recently implemented.[33] The narrow band ($\leqslant$1 MHz) infrared light is produced via cw nonlinear difference frequency mixing of visible, single mode Ar^+ (488 or 514.5 nm) and dye (R6G) lasers in a temperature controlled $LiNbO_3$ crystal[34] and split into reference and signal beams. The IR power on the reference beam is monitored with a photovoltaic, liquid N_2 cooled InSb infrared detector. The signal beam is multipassed 16 times via a Herriot cell through the modulated 4 cm long slit jet supersonic discharge and then focused onto a matched InSb detector. The signal and reference beams are then subtracted to eliminate common mode noise from Ar^+/dye laser fluctuations, resulting in a typical detection sensitivity of 10^{-6} $Hz^{-1/2}$, or $\approx 10^{-4}$ minimum absorbance in a 10 kHz detection bandwidth. This is already close to the shot noise limit, but can be further improved by high frequency concentration modulation methods, as described below.

The pulsed, slit supersonic discharge source can generate significant densities (typically$>10^{10}/cm^3$) of supersonically cooled molecular ions.[31] By switching the current through the discharge at 100 KHz, concentration modulation methods[33,35] can be employed to effectively discriminate against absorption signals from precursor species present in

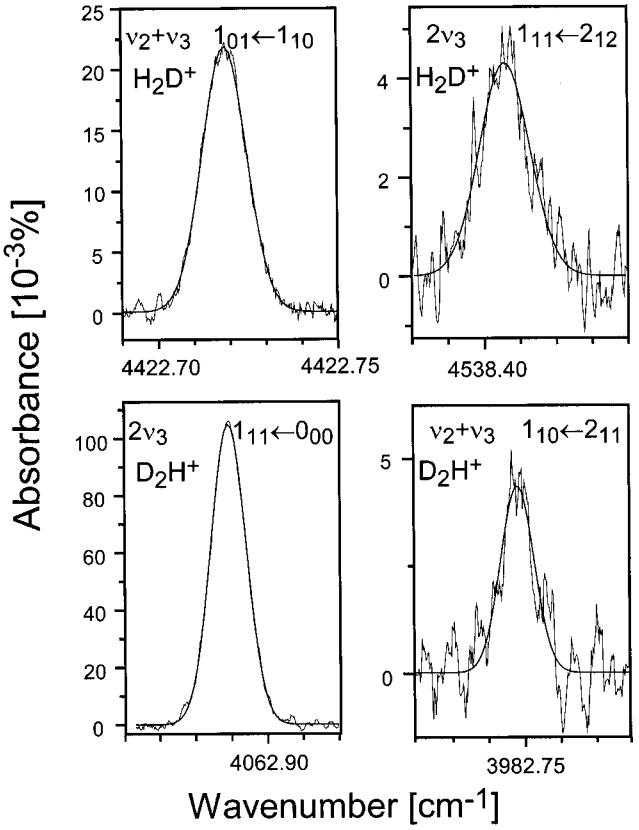

FIG. 1. Examples of overtone ($2\nu_3$) and combination band ($\nu_2+\nu_3$) absorption lines for H_2D^+ and D_2H^+ ions. Strongest and weakest absorption lines are shown to demonstrate the S/N dynamic range. Gaussian profiles are fitted through the experimental lines.

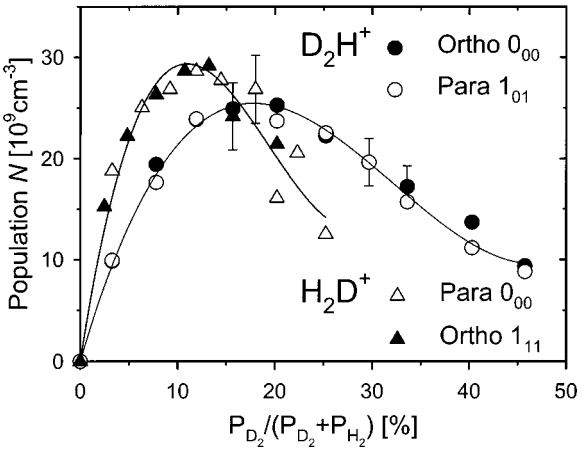

FIG. 2. Populations N of the lowest ortho (full symbols) and para (open symbols) states of H_2D^+ (triangles) and D_2H^+ (circles) ions as a function of the relative D_2 concentration in the expansion. Populations are obtained from ν_1 fundamental excitation on $2_{12}\leftarrow 1_{11}$ ($1_{01}\leftarrow 0_{00}$) for ortho (para) H_2D^+ and $1_{11}\leftarrow 0_{00}$ ($2_{12}\leftarrow 1_{01}$) for ortho (para) D_2H^+. The lowest H_2D^+ para state (0_{00}) population is scaled by fivefold to match the population of the lowest ortho state 1_{11}. Similarly, the lowest D_2H^+ para state (1_{01}) population is scaled by $\approx$1.5 to match the lowest ortho state 0_{00}.

orders of magnitude greater abundance. The implementation of lock-in detection at these high frequencies also provides additional noise discrimination, resulting in a detection sensitivity of about 4×10^{-7} $Hz^{-1/2}$. In a 3 KHz detection bandwidth, this corresponds to $\approx 2\times10^{-5}$ minimum absorbance per pulse, as previously demonstrated for H_3^+ ions.[33] This improvement in detection sensitivity proves to be crucial for the present experiment, where absorbances below 5×10^{-5} are routinely measured.

Figure 1 shows sample data scans over isolated rovibrational lines, demonstrating roughly the dynamic range of absorbances and S/N ratios for the strongest and weakest transitions observed in H_2D^+ and D_2H^+ ions. Note that peak absorbances are on the order 4×10^{-5} for the weakest lines. Center frequencies are obtained by least-squares fitting a Gaussian to the Doppler profiles. Relative frequencies are measured to better than $\approx$0.0001 cm^{-1} by monitoring dye laser transmission fringes through a stabilized Fabry–Perot optical transfer cavity,[36] to which the Ar^+ laser is servo loop locked as well. Absolute frequency calibration is achieved by referencing spectra[37] to the $R(0)$ line of HF at 4000.989 19 cm^{-1}, which is known to an accuracy better than 2×10^{-4} cm^{-1}.

The ions are formed in the discharge by adiabatically co-expanding a mixture of deuterium and hydrogen at a backing pressure of 300 Torr through the pulsed expansion slit (300 μm$\times$4 cm). The discharge current for optimum ion intensities is approximately 2 A, with D_2 and H_2 mole fractions varied to achieve maximum production efficiency for either H_2D^+ or D_2H^+ ion. Figure 2 shows the populations of the lowest ortho and para states of H_2D^+ and D_2H^+ ions as a function of the relative D_2 partial pressure, measured for four fundamental transitions. Note that absolute absorbances are measured, which from calculated transition strengths permits *absolute* populations of ions per quantum state to be reported. Although we defer kinetic interpretation of these curves until later in the discussion section, the optimum conditions for production of H_2D^+ ions are achieved with about a 10% mixture of D_2 in H_2, while for production of D_2H^+ ions the partial pressure of D_2 has to be increased to about 20%. In the previous studies of H_2D^+ or D_2H^+ the optimum conditions for production of these ions were at somewhat higher D_2 concentrations of approximately 20% for the H_2D^+ and 50% for the D_2H^+ production.[23,25] This observation is qualitatively consistent with the significantly lower rotational temperatures [$T_{rot}\approx 71(6)$ K] obtained in the present experiment compared to approximately 200 K and 150 K in previous studies.[23,25] as will be discussed in more detail in Sec. V. These data also permit relative populations of the jet-cooled nuclear spin manifolds to be determined directly, as indicated by the excellent agreement between suitably scaled versions of the ortho and para manifolds for both H_2D^+ and D_2H^+ (see Fig. 2).

Rotational temperatures of $T_{rot}\approx 71(6)$ K are characterized from Boltzmann plots, as shown in Fig. 3. These are in fact substantially higher than typically achieved in the slit jet discharge ($T_{rot}\approx 10-30$ K), due to the use of a predominantly H_2 expansion to maximize production of H_2D^+ or D_2H^+ ions. This avoids proton transfer loss to monatomic carrier gases such as Ar, although at the expense of less efficient rotational cooling with the light diatomic molecule diluent.

Theoretical calculations predict not only the line posi-

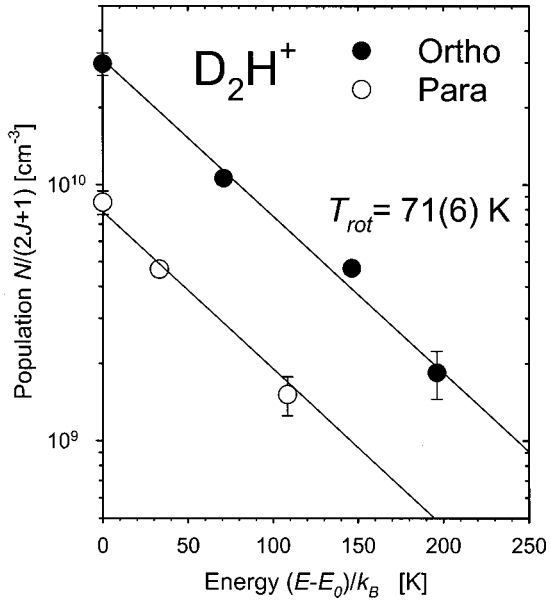

FIG. 3. Boltzmann plots as a function of initial state internal energy for the D_2H^+ ion. Full circles correspond to ortho states and open circles to para states. Both sets of data can be well described by a rotational temperature $T_{\rm rot}=71(6)$ K.

tions for H_2D^+ and D_2H^+ transitions, but also the line strengths. The line intensity measurements presented below confirm the reliability of these theoretical predictions, which can thus be used to estimate *absolute* state populations from measured integrated line absorbances. The experimental state populations so obtained are plotted as a function of the initial state internal energy in Boltzmann plots. In Fig. 3, two sets of populations for ortho states (full circles) and para states (open circles) are shown for the D_2H^+ ion, both fit to a rotational temperature of 71(6) K. The excellent agreement in Boltzmann slopes suggests that the ion rotational temperatures achieve thermal equilibrium in spite of the large asymmetric rotor spacings and less efficient cooling in diatomic hydrogen. This rotational temperature is also in good agreement with the translational temperature [$T\approx 61(5)$ K] measured along the laser beam via high-resolution Doppler linewidth analysis.

III. RESULTS: NON-BORN–OPPENHEIMER EFFECTS

Initial frequency and intensity predictions for these studies are based on the non-Born–Oppenheimer potentials of Dinelli *et al.*,[29] which had been refined using spectroscopy data available at the time. Intensities were calculated using the dipole surface of Röhse *et al.*[38] During the analysis of the present data, however, new *ab initio* frequency predictions were made. Although a detailed description of these non-Born–Oppenheimer calculations is addressed elsewhere,[30] the essential ideas can be quickly summarized. These calculations start with high accuracy *ab initio* electronic structure efforts [$V_{ab\ initio}(Q)$] augmented with relativistic corrections [$V_{\rm rel}(Q)$] to yield a state-of-the art Born–Oppenheimer surface,[39] i.e., $V_{\rm BO}(Q)=V_{ab\ initio}(Q)+V_{\rm rel}(Q)$, which is then further modified to model mass dependent non-Born–Oppenheimer effects. First of all, the so-called ''adiabatic'' or diagonal corrections to the Born–Oppenheimer potential surface are included, which yield

$$V(Q)=V_{\rm BO}(Q)+\frac{1}{\mu^S}\Delta V^S_{\rm ad}(Q)+\frac{1}{\mu^A}\Delta V^A_{\rm ad}(Q). \qquad (2)$$

The $\Delta V^S_{\rm ad}(Q)$ symmetric adiabatic term is the only nonvanishing term for *symmetric* isotopomers (e.g., D_3^+,H_3^+), with a mass factor of $(\mu^s)^{-1}=\Sigma_i 1/m_i$. Conversely, for *asymmetrically* substituted ions such as D_2H^+ and H_2D^+, there is an additional correction term, $\Delta V^A_{\rm ad}(Q)$, with $(\mu^A)^{-1}=1/m_a-1/m_b$, where m_a and m_b refer to the unique versus doubly present H/D atoms, respectively.

However, modifying the potential surface with mass dependent terms is not sufficient. In order to implement this approximate non-Born–Oppenheimer model, the kinetic energy operator is also rewritten in a form that explicitly allows different masses for rotational and vibrational motion. As supported by detailed studies of diatomic non-Born–Oppenheimer effects for H_2 and H_2^+ by Bunker and Moss,[40,41] the rotational masses in the kinetic energy operator are taken to be the exact *nuclear* masses of the various H versus D isotopes (i.e., excluding the electron mass). The effective vibrational mass for each isotope is similarly obtained from the H_2 and H_2^+ results of Moss,[42,43] which yield $m_{\rm H}$, $m_{\rm D}$ values intermediate between a bare nucleus and full atomic mass. Nonadiabatic effects are then incorporated by solving for eigenvalues of this non-Born–Oppenheimer corrected potential and kinetic energy operator Hamiltonian with variational calculations. Numerical convergence of these calculations is better than 0.005 cm^{-1}, i.e., safely beyond the limits due to either experiment uncertainty or residual non-Born–Oppenheimer contributions unaccounted for in the present model.

The spectral search for overtone rovibrational transitions in H/D substituted H_3^+ reveals 16 lines of D_2H^+ and 8 lines of H_2D^+ ions [see Figs. 4(a) and 4(b)], greatly accelerated by theoretical predictions. Indeed, all measured lines are found near to the predicted position (see Tables I and II), effectively eliminating long spectral searches for each ion with sparse transitions extending over $\approx$300 cm^{-1}. The theoretical calculations also yield transition strengths, which allow the scans to concentrate on lines with intensities predicted above experimental sensitivity limits. Attempts to observe several transitions with intensities below these limits yield negative results, confirming the qualitative reliability of the theoretical predictions. Figure 5 shows a sample scan region, which reveals two close transitions of D_2H^+ ion together with the predicted positions indicated by the arrows. Each transition in the present data set has been scanned repeatedly (3 to 9 times) to confirm both relative frequencies and intensities. Intensity data measured over multiple days of experimentation are normalized to multiple reference peaks.

Tables I and II summarize the line positions for D_2H^+ and H_2D^+ ion, respectively. As the primary interest in these H_2D^+ and D_2H^+ species relates to rigorous high-resolution tests of non-Born–Oppenheimer effects, we defer discussion of the spectral assignment and analysis until later in the discussion and instead focus on comparison between theory and

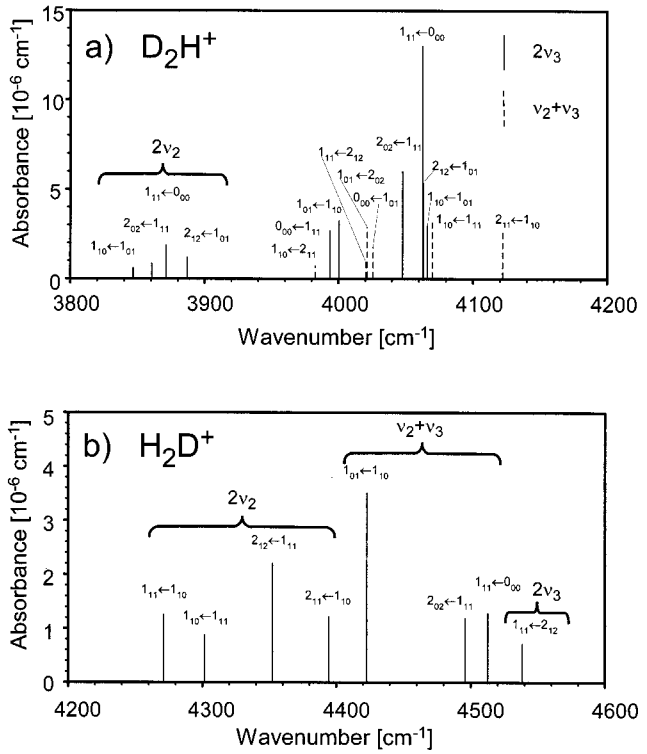

FIG. 4. Overview of jet-cooled overtone ($2\nu_2$,$2\nu_3$) and combination ($\nu_2+\nu_3$) band spectra for D_2H^+ (a) and H_2D^+ (b).

experiment. Also listed in Tables I and II are the deviations between the experimentally measured line positions and the spectral predictions reflecting semiempirical and *ab initio* treatment of non-Born–Oppenheimer effects. The second, more accurate set of predictions is based on the use of the ultrahigh accuracy *ab initio*+relativistic potential surface,[39] including both symmetric and asymmetric ''adiabatic'' corrections to $V(Q)$ as well as explicit non-Born–Oppenheimer kinetic energy operator terms.

The data indicate several interesting trends. First of all, there is an overall remarkable level of agreement between theory and experimental results, with maximal discrepancies of only ≈ 0.2 cm^{-1} for the semiempirical and less than 0.1 cm^{-1} for the *ab initio* predictions. In fact, the majority of the predicted frequencies are within 0.04 cm^{-1} of the experimental data. By way of example, sample data and theoretical predictions are shown in Fig. 5 for two overtone transitions in the $2\nu_3$ manifold of D_2H^+, where the arrows below (above) the frequency axis refer to the semiempirical (*ab initio*) set of predictions, respectively. Indeed, the second set of fully *ab initio* predictions shows roughly an additional order of magnitude increase in accuracy, with a typical prediction error of ≈ 0.05 cm^{-1} and in line with previous studies.[30] Although still significantly outside the range of experimental uncertainties (≈ 0.001 cm^{-1}), these results should be compared with intrinsic non-Born–Oppenheimer correction terms on the order of $\approx$several cm^{-1}. This confirms that the non-Born–Oppenheimer models employed are achieving near spectroscopic levels of accuracy, even for overtone transitions in the asymmetrically substituted isotopomers.

Second, the deviations between semiempirical predictions and experiment exhibit a systematic dependence on the molecular vibrations involved. For H_2D^+, for example, the deviations are all positive (≈ 0.14 cm^{-1}) for $2\nu_2$, negative (≈ -0.15 cm^{-1}) for $2\nu_3$, and close to zero ($\approx \pm 0.021$ cm^{-1}) for the combination band $\nu_2+\nu_3$. For D_2H^+, the non-Born–Oppenheimer effects reverse, as might be expected from the inverted nature of the isotopically substituted D versus H atoms. For example, the discrepancies are systematically negative (≈ -0.04 cm^{-1}) for $2\nu_2$. The corresponding non-

TABLE I. Observed λ_{exp} line positions and their deviations $\delta=\lambda_{exp}-\lambda_{calc}$ from calculated values λ_{calc} for D_2H^+.

			Wave number [cm^{-1}]		
Ortho/para	Vibration	$J'_{K_{a'}K_{c'}} \leftarrow J''_{K_{a''}K_{c''}}$	λ_{exp}	δ^a	δ^b
p	$2\nu_2$	$1_{10} \leftarrow 1_{01}$	3846.7864(43)	−0.040	−0.023
o	$2\nu_2$	$2_{02} \leftarrow 1_{11}$	3860.6596(30)	−0.039	−0.017
o	$2\nu_2$	$1_{11} \leftarrow 0_{00}$	3871.3773(13)	−0.046	−0.030
p	$2\nu_2$	$2_{12} \leftarrow 1_{01}$	3887.0520(21)	−0.039	−0.017
o	$2\nu_3$	$0_{00} \leftarrow 1_{11}$	3993.5179(9)	0.207	−0.033
p	$2\nu_3$	$1_{10} \leftarrow 1_{01}$	4066.1576(9)	0.204	−0.046
p	$2\nu_3$	$1_{01} \leftarrow 1_{10}$	4000.4940(8)	0.127	−0.034
o	$2\nu_3$	$2_{02} \leftarrow 1_{11}$	4047.8403(4)	0.130	0.002
o	$2\nu_3$	$1_{11} \leftarrow 0_{00}$	4062.8893(2)	0.083	−0.044
p	$2\nu_3$	$2_{12} \leftarrow 1_{01}$	4062.9832(5)	0.087	−0.032
o	$\nu_2+\nu_3$	$1_{10} \leftarrow 2_{11}$	3982.7480(41)	−0.075	−0.003
p	$\nu_2+\nu_3$	$0_{00} \leftarrow 1_{01}$	4025.8734(14)	−0.075	−0.023
o	$\nu_2+\nu_3$	$1_{10} \leftarrow 1_{11}$	4069.8581(8)	−0.075	−0.033
p	$\nu_2+\nu_3$	$1_{11} \leftarrow 2_{12}$	4020.5342(27)	0.005	−0.040
p	$\nu_2+\nu_3$	$2_{11} \leftarrow 1_{10}$	4121.7757(9)	0.026	−0.035
o	$\nu_2+\nu_3$	$1_{01} \leftarrow 2_{02}$	4021.2350(9)	0.050	−0.042

[a]Calculated line position λ_{calc} using spectroscopically determined potentials.
[b]λ_{calc} from *ab initio* calculations.

TABLE II. Observed λ_{exp} line positions and their deviations $\delta=\lambda_{exp}-\lambda_{calc}$ from calculated values λ_{calc} for H_2D^+.

Ortho/para	Vibration	$J'_{K_{a'}K_{c'}} \leftarrow J''_{K_{a''}K_{c''}}$	Wave number [cm^{-1}]		
			λ_{exp}	δ^a	δ^b
o	$2\nu_2$	$1_{11}\leftarrow 1_{10}$	4271.0174(11)	0.142	−0.078
o	$2\nu_2$	$1_{10}\leftarrow 1_{11}$	4301.6315(17)	0.138	−0.089
o	$2\nu_2$	$2_{12}\leftarrow 1_{11}$	4352.3589(7)	0.141	−0.071
o	$2\nu_2$	$2_{11}\leftarrow 1_{10}$	4394.3288(11)	0.129	−0.082
o	2_{ν_3}	$1_{11}\leftarrow 2_{12}$	4538.4054(24)	−0.149	0.034
o	$\nu_2+\nu_3$	$1_{01}\leftarrow 1_{10}$	4422.7188(4)	0.021	0.013
o	$\nu_2+\nu_3$	$2_{02}\leftarrow 1_{11}$	4495.8809(11)	−0.007	0.037
p	$\nu_2+\nu_3$	$1_{11}\leftarrow 0_{00}$	4512.5665(11)	0.016	0.013

[a]Calculated line position λ_{calc} using spectroscopically determined potentials.
[b]λ_{calc} from *ab initio* calculations.

Born–Oppenheimer effects for $2\nu_3$ and $\nu_2+\nu_3$ vibrations are more difficult to infer, as the predictions are also influenced by strong *C* axis Coriolis coupling between the two near resonant manifolds. However, if only transitions to the Coriolis unperturbed states ($J'_{K'_aK'_c}=0_{00}$ and 1_{10}) are considered, deviations for $2\nu_3$ are consistently positive ($\approx+0.2$ cm^{-1}), whereas the $\nu_2+\nu_3$ band yields discrepancies closer to zero (≈ -0.075 cm^{-1}). These reflect vibrational and isotopic trends that are not completely accounted for in what are effectively extrapolations of the fits of Dinelli *et al.*[29] Conversely, the *ab initio* predictions yield a significant improvement in precision modeling of non-Born–Oppenheimer interactions. Now the agreement between theory and experiment is improved to $\approx$0.03–0.04 cm^{-1}, which captures all rovibrationally non-Born–Oppenheimer effects at nearly spectroscopic levels of accuracy. These results demonstrate that the *ab initio* calculations extrapolate to new spectral regions much more reliably than results based on high quality fits to previously observed spectra. The information gained in these experiments will be used to further refine theoretical models of non-Born–Oppenheimer effects.[44]

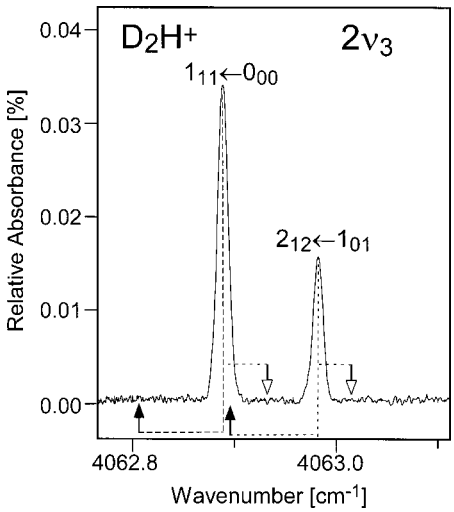

FIG. 5. An experimental scan over two lines corresponding to $2\nu_3$ $1_{11}\leftarrow 0_{00}$ and $2_{12}\leftarrow 1_{01}$ transitions in D_2H^+ ion. Full and open arrows indicate theoretical predictions based on semiempirical and *ab initio* non-Born–Oppenheimer model treatments, respectively. See text for more details.

IV. SPECTRAL ASSIGNMENT AND ANALYSIS: CORIOLIS INTERACTIONS

Though a primary impetus for the present work has been an experimental test of the *ab initio* non-Born–Oppenheimer calculations, these spectra presented herein also reflect first high-resolution data on H_2D^+ and D_2H^+ in the overtone and combination band region. Due to large rotational constants and efficient cooling in the slit jet discharge, the spectra are extremely sparse, with only the very lowest energies ($J=0,1$, and a few $J=2$ levels) populated sufficiently to detect, and no internal combination differences for independent spectroscopic confirmation of a given assignment. Furthermore, due to the exclusive presence of light H/D atoms in the ions, these overtone/combination band vibrations correspond to large amplitude motion, which leads to anomalously strong vibration/rotation mixing effects. On the other hand, the theoretical predictions specify the two good quantum numbers: rotational state *J* and nuclear spin symmetry (ortho/para). Thus zero order assignment of these bands as $J_{K_aK_c}$ rovibrational transitions is relatively straightforward for less perturbed vibrational states such as $2\nu_2$ of D_2H^+, whose energy levels can therefore be adequately described as a rigid asymmetric top. However, this situation becomes more complicated for the $2\nu_3$ and $\nu_2+\nu_3$ modes, which are near resonant with each other and therefore exhibit strong Coriolis mixing effects described below.

Both the H_2D^+ and D_2H^+ ions belong to the C_{2v} symmetry group and the three normal vibrational modes: a symmetric "breathing" mode ν_1, a bending mode ν_2, and an asymmetric stretch ν_3, with symmetries of A_1, A_1, and B_2, respectively. Thus by standard group theoretical analysis, both the $2\nu_2$ and $2\nu_3$ overtone states (each A_1) can interact with the $\nu_2+\nu_3$ combination band vibration (B_2) via *C*-axis Coriolis coupling, yielding selection rules of $\Delta J=0$, $\Delta K_a=$ odd, and $\Delta K_c=$ even. This implies that 0_{00} and 1_{10} states are unperturbed, whereas each of the (1_{01},1_{11}), (2_{11},2_{21}), and (2_{02},2_{12},2_{20}) states can form strongly Coriolis coupled pairs and triplets. To facilitate spectroscopic assignment of individual transitions in D_2H^+ and H_2D^+ ions, the molecules are therefore approximated as rigid asymmetric tops with Coriolis coupling included via two (or three) state perturbation theory. The rigid asymmetric top molecular con-

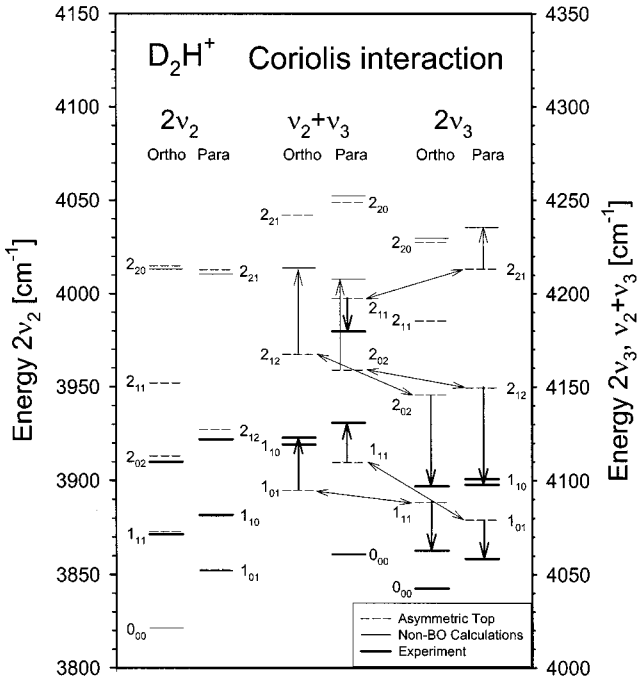

FIG. 6. Predicted term values for D_2H^+: the zero order asymmetric top energy levels (dashed lines) are strongly pushed (solid heavy one-directional arrows) by *C*-axis Coriolis coupling (solid light double-sided arrows) into excellent agreement with experimentally observed (heavy lines) and theoretically predicted term values (light full lines) for $2\nu_3$ and $\nu_2+\nu_3$ vibrations. For the $2\nu_2$ vibration, which is far off resonance ($\approx$200 cm^{-1}) with $\nu_2+\nu_3$, the experimental and theoretically predicted term values agree well with simple zero-order asymmetric top predictions. Note the offset in frequency axis for $2\nu_2$ (left), and $2\nu_3$ and $\nu_2+\nu_3$ (right).

stants *A*, *B*, and *C* for overtone and combination vibrations can be estimated by linear extrapolation from

$$X_{\nu_1,\nu_2,\nu_3}=X_e-\Sigma\,\alpha_i(\nu_i+1/2), \tag{3}$$

where *X* stands for *A*, *B*, and *C*; the equilibrium constant X_e and coefficients α_i can be evaluated from the ground state and the first excited state constants for each molecular ion and vibration.[24,26] Zero order deperturbed energy levels for the Coriolis coupled states are then estimated from simple rigid top formula and predicted band origins. The rotational dependence of *C*-axis coupling matrix elements is diagonal in *K* and therefore $\approx\gamma K_c$ for a near oblate symmetric top, where γ depends only on the vibrational states and therefore is approximately the same for each Coriolis pair or triplet. With least-squares selection of γ, this permits term values for each of the Coriolis coupled states to be predicted from simple 2×2 or 3×3 matrix diagonalization.

The predictions for D_2H^+ are shown in Fig. 6 and fully support the Coriolis analysis presented above. The zero order asymmetric top energy levels (dashed lines) are strongly shifted by *C*-axis Coriolis coupling (arrows) into excellent agreement with the experimentally observed and theoretically predicted term values (full lines). Note that the magnitude of the coupling ($\gamma\approx30\ cm^{-1}$) is greater than the difference in band origins ($\Delta\nu_0\approx18\ cm^{-1}$) and indeed "inverts" the zero order asymmetric top level structure in several notable instances (e.g., in $\nu_2+\nu_3$, $E_{2_{12}}>E_{2_{02}}>E_{2_{11}}$ and in corresponding $2\nu_3$ $E_{1_{10}}>E_{2_{12}}>E_{2_{01}}$). This extensive degree of mixing makes an assignment of $J_{K_aK_c}$ quantum numbers only approximate, but these labels are nevertheless useful to characterize the predominant parentage in the zero order states.

For H_2D^+ ion a similar analysis has been made, although with fewer transitions measured as a result of the lower ion concentrations. The $2\nu_3$ and $\nu_2+\nu_3$ modes are again strongly Coriolis mixed; the magnitude of the coupling ($\gamma\approx40\ cm^{-1}$) is comparable to that observed in D_2H^+, though with smaller effect due to a much larger difference in band origins ($\Delta\nu_0\approx140\ cm^{-1}$ versus 18 cm^{-1}). Only $\approx$10–30 cm^{-1} Coriolis shifts are observed, qualitatively preserving the conventional asymmetric top energy level pattern.

V. LINE STRENGTHS AND STATE POPULATIONS

Absorption based measurements also yield valuable complementary information on lower state populations via line intensities. Although experimental line strengths are typically determined far less precisely than spectral line positions, repeated scans over transitions can be used to yield *relative* line strengths to $<$10% accuracy. These relative overtone versus fundamental line intensities can then be compared to theoretical calculations and thereby provide independent assessment of the *ab initio* dipole moment surface at large amplitude vibrational displacement.

The measured integrated absorbance is given by

$$A=N_0\cdot l\cdot I(\omega_{if}), \tag{4}$$

where N_0 is the molecule density in the region and $l=64$ cm is the total absorption path length. The transition factor $I(\omega_{if})=S_0\times P_i$ is a product of line strength S_0 and lower state population (upper state populations are negligible at these temperatures)

$$P_i=\frac{Q_{\rm NS}\cdot Q_J}{Q_R}e^{-E_i/kT_{\rm rot}}, \tag{5}$$

where $Q_{\rm NS}$ is the nuclear spin weight factor ($Q_{\rm NS}=3$ and 1 for ortho and para states, respectively, in H_2D^+, and 6 and 3 for ortho and para states, respectively, in D_2H^+), $Q_J=(2J+1)$ is the rotational degeneracy, and Q_R is the rotational partition function. The exponential Boltzmann factor depends on the rotational term energy E_i and the rotational temperature $T_{\rm rot}$. From substitution of $I(\omega_{if})$ into Eq. (4), the population of a given initial state $N_i=N_0\ P_i$ can be evaluated from the experimental absorbance and the theoretically predicted line strength S_0:

$$N_i=\frac{A}{S_0\cdot l}. \tag{6}$$

Figure 7 displays populations divided by the rotational degeneracy $N_i/(2J+1)$ for various lower rotational states evaluated from different overtone and fundamental rovibrational transitions. The key point of this plot is that populations inferred via transitions originating from the *same* lower state should obviously be identical; the degree of agreement therefore reflects the accuracy with which theoretical calcu-

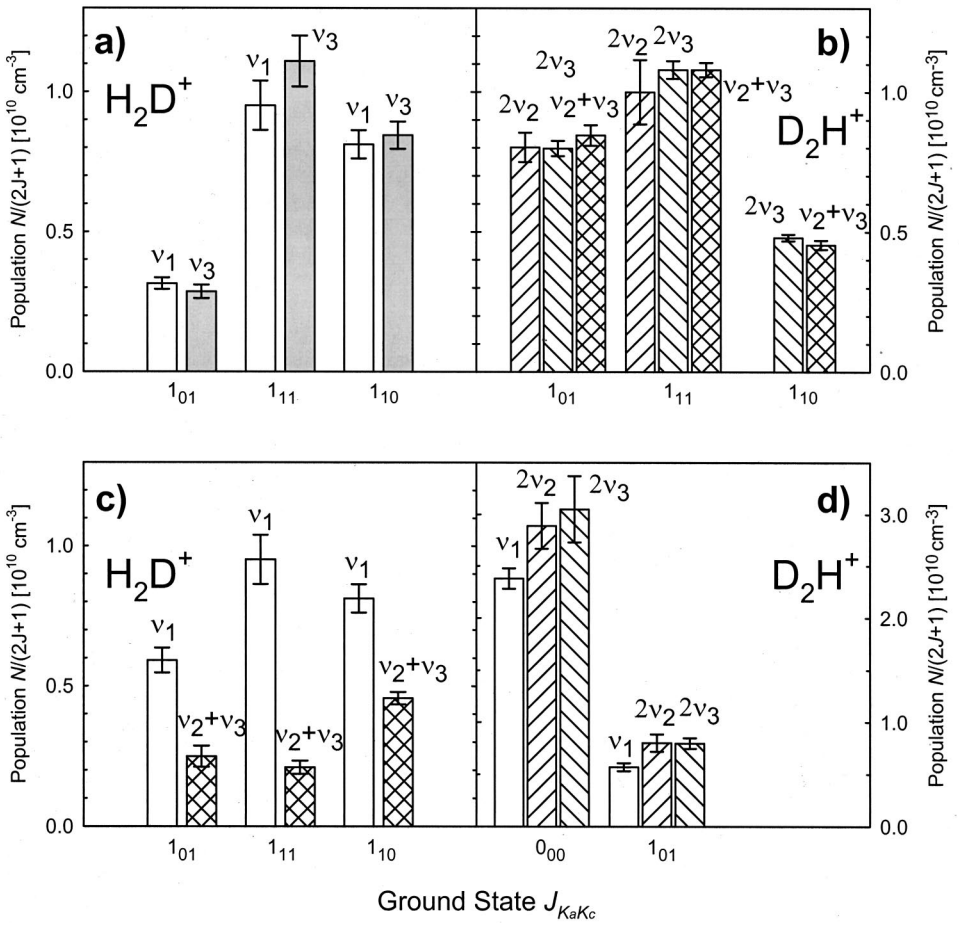

FIG. 7. State populations inferred from different vibrational transitions for H_2D^+ and D_2H^+ ions: (a) fundamental ν_1 and ν_3 vibrational transitions for H_2D^+ ion; (b) overtone $2\nu_2$ and $2\nu_3$, and combination $\nu_2+\nu_3$ vibrational transitions for D_2H^+ ion; (c) fundamental ν_1 and combination $\nu_2+\nu_3$ vibrational transitions for H_2D^+; and (d) fundamental ν_1 and overtone $2\nu_2$ and $2\nu_3$ vibrational transitions for D_2H^+.

lations predict the line strength S_0. One can also isolate and test the rotational dependence of these rovibrational transitions for a given vibrational state. Indeed, the rotational dependence of both experimental and theoretical line strengths is found to be in relatively good agreement (≈20%) with rigid asymmetric rotor calculations.[45] Figure 7 is therefore restricted to lower state populations evaluated from a series of vibrational transitions, which in effect focuses on the accuracy of the dipole moment derivative surface.

Figure 7(a) isolates several pairs of transitions from different fundamental ν_1 and ν_3 vibrational transitions for the H_2D^+ ion. In general, there is very good overall agreement between rotational populations inferred from each pair. The greater abundance of 1_{11} and 1_{10} levels with respect to the lower energy 1_{01} level reflects the higher population of *ortho* versus *para* states caused by nuclear spin statistics, which will be discussed in more detail in the following section. Similarly, Fig. 7(b) demonstrates excellent agreement between populations evaluated from different overtone $2\nu_2$ and $2\nu_3$, and combination $\nu_2+\nu_3$ vibrational transitions for the D_2H^+ ion. All populations agree within the experimental uncertainty obtained from repeated measurements. This level of agreement provides good support for the high quality of both the *ab initio* surface and dynamical calculations.

On the other hand, significant discrepancies are revealed in populations obtained by comparison between fundamental versus combination [see Fig. 7(c)] and overtone [see Fig. 7(d)] transitions for H_2D^+ and D_2H^+ ion, respectively. The populations evaluated from combination $\nu_2+\nu_3$ vibrational transitions are 40–60 % *lower* than the corresponding populations evaluated from fundamental ν_1 transitions for H_2D^+ ion in Fig. 7(c). Conversely, populations evaluated from overtone $2\nu_2$ and $2\nu_3$ vibrational transitions for D_2H^+ [see Fig. 7(d)] are approximately 30% *higher* than those evaluated from fundamental ν_1 transitions. It is worth noting that populations inferred from these overtone transitions are consistent with $\nu_2+\nu_3$ [see Fig. 7(b)], and thus similar discrepancies must also exist between fundamental and combination band vibrations in D_2H^+.

This level of disagreement is real and will be the subject of further *ab initio* studies. It is worth noting that the present comparison is based on intensities derived from the less accurate semiempirical wave functions and dipole surfaces, which have since been superceded.[39] Given that the semiempirical predictions for eigenfrequencies are still quite accurate, the dipole surface would seem the more plausible source of such discrepancies. In this regard, the line strength S_0 of a given transition derives from the transition dipole matrix element $\langle \Psi_f | \boldsymbol{\mu} | \Psi_i \rangle$, which is conventionally represented by a Taylor series expansion of dipole moment derivatives of $\boldsymbol{\mu}(Q)$:

$$\boldsymbol{\mu}(Q)=\boldsymbol{\mu}(Q_e)+\sum_i \frac{\partial \boldsymbol{\mu}}{\partial Q_i}\cdot Q_i+1/2\sum_{i,j}\frac{\partial^2 \boldsymbol{\mu}}{\partial Q_i \partial Q_j}Q_iQ_j + \cdots . \quad (7)$$

TABLE III. Ion–molecule reactions, enthalpies, and rate coefficients considered in a plasma chemistry model for the slit expansion discharge ion source.

Reaction		Reaction enthalpy ΔH^a $[cm^{-1}]$	Reaction rate coefficient $[10^{-10}\ cm^3 s^{-1}]$		
			T [K]	300[b]	71[c]
$H_2^+ + D_2 \rightarrow D_2H^+ + H_2$	(i)	−237	k_1	10	11
$H_3^+ + D_2 \rightarrow H_2D^+ + HD$	(ii)	−105	k_2	2.6	3.5
$D_2H^+ + H_2 \rightarrow H_2D^+ + HD$	(iii)	132	k_3	5.7	2.4
$D_2H^+ + D_2 \rightarrow D_3^+ + HD$	(iv)	−106	k_4	5.2	8.7
$H_2D^+ + H_2 \rightarrow H_3^+ + HD$	(v)	163	k_5	5.3	2.0
$H_2D^+ + D_2 \rightarrow D_2H^+ + HD$	(vi)	−74	k_6	6.5	7.0
$H_2D^+ + D_2 \rightarrow D_3^+ + H_2$	(vii)	−238	k_7	3.5	7.0
$D_3^+ + H_2 \rightarrow D_2H^+ + HD$	(viii)	164	k_8	2.9	1.7
$D_2H^+ + H_2 \rightarrow H_3^+ + D_2$	(ix)	237	k_{-1}	1.9	0.0
$D_3^+ + H_2 \rightarrow H_2D^+ + D_2$	(x)	238	k_{-7}	5.3	0.0

[a]Reaction enthalpies calculated using zero-point energies of Carney (Ref. 47) and of Huber and Herzberg (Ref. 48).

[b]All the rate coefficients at 300 K from Ref. 46.

[c]Rate coefficients for exoergic reactions (k_1, k_2, k_4, k_6, and k_7) at 71 K taken as reported at 80 K in Ref. 46, strongly endothermic reaction rates (k_{-1} and k_{-7}) set to zero, k_5 fixed at theoretical value (Ref. 49), with k_3 and k_8 least-squares fitted to the experimental data (see text for details).

In this approximation, vibrational intensities in the fundamental bands are dominated by the lowest (i.e., first order) partial derivatives with respect to each normal mode coordinate. Intensities in overtone/combination bands are governed by both first and second order partial derivatives and are therefore more sensitive to deviations in the shape of the dipole moment surface farther from the origin. This provides at least a plausibility argument for why transition strengths, internally consistent among the fundamental vibrations [Fig. 7(a)] and among the overtone and combination vibrations [Fig. 7(b)], could nevertheless result in discrepancies between the fundamental and the higher order vibrational excitations.

As a second observation, the experimentally measured population (i.e., transition strength) discrepancies occur in *opposite* directions for H_2D^+ and D_2H^+ ions [see Figs. 7(c) and 7(d)]. For example, when normalized to the overtone and combination bands, the ν_1 fundamental based populations appear to be overestimated for H_2D^+ and underestimated for D_2H^+. Without an independent measure of these populations, one cannot uniquely determine whether this is due to an error in the fundamental or overtone/combination band transition strengths or both. However, a plausible model for this can be developed from a simple normal mode analysis. Specifically, the ν_1 vibration in D_2H^+ corresponds predominantly to stretching of the ''unique'' (i.e., H) atom with only minor extension of the ''nonunique'' (i.e., D–D) diatomic pair. Conversely, this mode description is qualitatively reversed in H_2D^+, for which ν_1 largely reflects the symmetric extension of the nonunique H–H atom pair with only minimal stretching of the unique D atom. Once account is taken of shifts in the center of mass, this provides a plausible explanation for the observed discrepancies in fundamental versus overtone transition strengths and/or inferred populations. For example, if dipole moment derivatives on the surface are overpredicted for radial extension of a single atom versus symmetric stretching of the diatom pair, this would nicely account for the observed reversal with isotopic substitution. In any event, these results clearly reveal small but finite errors in higher order dipole surface derivatives, which would therefore be a worthwhile target for further theoretical investigation.

VI. ION–MOLECULE REACTIONS AND ORTHO/PARA POPULATION ANALYSIS

These population data provide additional insights into ion–molecule kinetics of jet-cooled species and ortho–para interconversion dynamics in the discharge slit expansion. Figure 2 shows the populations of the lowest ortho and para states of H_2D^+ and D_2H^+ ions as a function of the fractional D_2 concentration in the stagnation region. The populations are all obtained from fundamental excitations on following rotational transitions: $2_{12} \leftarrow 1_{11}$ ($1_{01} \leftarrow 0_{00}$) transition for ortho (para) H_2D^+, and $1_{11} \leftarrow 0_{00}$ ($2_{12} \leftarrow 1_{01}$) transition for ortho (para) D_2H^+. Although these measurements are performed to optimize the expansion conditions for a particular isotopomeric ion, they also contain interesting information about low temperature ion–molecular chemistry in the discharge source, as described below.

Since H_2 dominates in the slit discharge source, the chain of ion–molecule reactions starts with molecular hydrogen ionization to form H_2^+, which rapidly reacts with molecular hydrogen to form H_3^+, reaction (1). This is then followed by subsequent reaction of H_3^+ ions with D_2 to produce H_2D^+ and D_2H^+:

$$H_3^+ + D_2 \rightarrow D_2H^+ + H_2, \tag{8a}$$

$$\rightarrow H_2D^+ + HD. \tag{8b}$$

These ion concentrations then evolve by a series of reactions with H_2 and D_2 molecules, the previously measured rate data for which are summarized in Table III. Most generally stated, the overall scheme can be written in terms of eight forward/backward reactions representing each of the four ions (H_3^+, H_2D^+, D_2H^+, D_3^+) reacting with each of the two reagents

(H_2,D_2), where each of the forward/backward reaction pairs is rigorously constrained by detailed balance. However, the full set of reactions is more general than necessary for our case, since HD concentrations are extremely small in the discharge, limited primarily by natural isotope abundance and/or ion–molecular formation rates in the discharge. This translates into 3 to 4 orders of magnitude lower [HD] than $[H_2]$ or $[D_2]$ and therefore reactions consuming HD as reagent can be safely neglected. Thus the set of eight relevant reaction pairs can be conveniently organized into *non-HD producing* reactions,

$$H_3^+ + D_2 \leftrightarrow D_2H^+ + H_2, \quad \text{(i)}$$

$$H_2D^+ + D_2 \leftrightarrow D_3^+ + H_2, \quad \text{(vii)}$$

and *HD producing* reactions,

$$H_3^+ + D_2 \leftrightarrow H_2D^+ + HD, \quad \text{(ii)}$$

$$D_2H^+ + H_2 \leftrightarrow H_2D^+ + HD, \quad \text{(iii)}$$

$$D_2H^+ + D_2 \leftrightarrow D_3^+ + HD, \quad \text{(iv)}$$

$$H_2D^+ + H_2 \leftrightarrow H_3^+ + HD, \quad \text{(v)}$$

$$H_2D^+ + D_2 \leftrightarrow D_2H^+ + HD, \quad \text{(vi)}$$

$$D_3^+ + H_2 \leftrightarrow D_2H^+ + HD, \quad \text{(viii)}$$

where the numbering of equations is consistent with the rate constant labels in Table III. [Note that two additional rate processes are in included in Table III to consider reverse reaction pathways for (i) and (vii).] Consequently, we need only two pairs of forward/reverse rate constants from the first set (k_1,k_{-1},k_7,k_{-7}) and the six forward rate constants from the second set $(k_2,k_3,k_4,k_5,k_6,k_8)$ to describe the kinetics completely, where any pair of reaction rate constants is necessarily constrained by detailed balance considerations.

Given the long-range nature of the proton transfer kinetics, these reactions proceed at close to Langevin rates and therefore quickly permit the ion concentrations to reach steady state levels. For example, an ion–molecule reaction with $k \approx 10^{-9}-10^{-10}$ cm^3 s^{-1} has a $1/e$ time of $\approx$30–300 ns for typical reagent H_2 concentrations in the slit jet expansion ($\approx 3\times10^{16}$ cm^{-3}). As the H_2D^+ and D_2H^+ ions are probed by the IR laser multipass about 5 mm (i.e., ≈ 5 μs) downstream from the valve orifice, the ions have undergone $\approx$10–200 reaction cycles and thereby achieve *steady state* conditions prior to detection. ''Ion catalyzed conversion'' of H_2/D_2 into HD executes only one cycle per $1/e$ ion–molecule lifetime, which therefore yields negligible build up of product HD on the 5 μs time scale, both with respect to H_2/D_2 as well as HD in natural abundance. Total H_2D^+ and D_2H^+ ion concentrations as a function of relative D_2 concentration are obtained from the experimentally measured populations in Fig. 2 by summing over all quantum states, based on a least-squares-fit Boltzmann temperature of 71(6) K (see Fig. 3). The experimental populations for H_2D^+ and D_2H^+ are shown in Fig. 8. These total ion concentrations peak at about 12% and 18% fractional D_2 concentration for H_2D^+ and D_2H^+ ions, respectively, with a maximum D_2H^+ concentration about 1.5 higher than the corresponding maximum in H_2D^+ concentration.

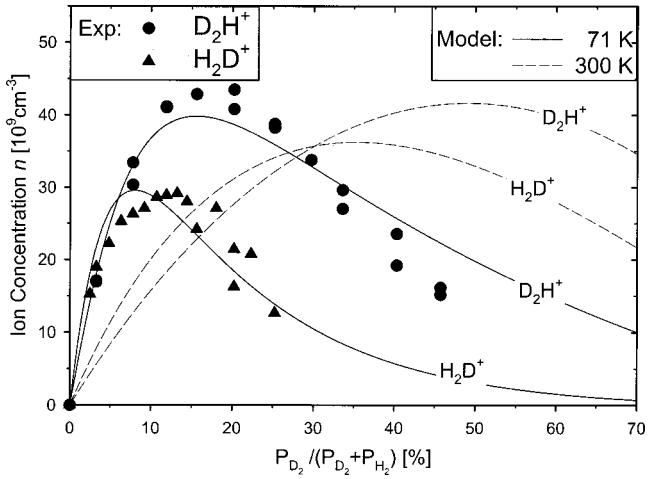

FIG. 8. Total ortho/para H_2D^+ (triangles) and D_2H^+ (circles) ion concentrations as a function of relative D_2 concentration. Kinetic simulations of ion concentrations using a steady state model, Eq. (7), with rate coefficients summarized in Table III for 300 K (dashed lines) and 71 K (solid lines) are shown.

As the simplest kinetic analysis of this data, we explore a steady state model to investigate this dependence of total D_2H^+ and H_2D^+ concentrations on D_2 mole fraction in the discharge region. Reaction rates for each of the ion–molecule reactions considered are obtained from the VT–SIFT measurements of Giles *et al.*,[46] which report rate coefficients at temperatures of 80 K and 300 K (see Table III). These two temperature sets of rate constants are then used to solve for relative ion concentrations of D_2H^+ and H_2D^+ as a function of D_2/H_2 mole fraction, setting time derivatives of all ion species to zero. The theoretical steady state results for 300 K are shown in Fig. 8 and clearly predict that maximum H_2D^+ and D_2H^+ ion production requires much *higher* D_2 concentrations than experimentally observed at 71 K. Specifically, the predicted H_2D^+ and D_2H^+ concentrations at 300 K peak for $X_{D_2} \approx 0.35$ and 0.50, respectively, which is in reasonable agreement with values observed in previous ''high temperature'' studies at 200 K and 150 K.[23,25] Also relevant is the significant *decrease* in optimal D_2 mole fractions ($X_{D_2} \approx 0.17$ and 0.33 for H_2D^+ and D_2H^+, respectively) suggested from the low temperature rate constants[46] obtained in VT–SIFT experiment at 80 K (omitted from Fig. 8 for clarity). Indeed, such trends are in good qualitative agreement with the current experimental data at even lower temperatures [71(6) K], which yield peak concentrations of H_2D^+ and D_2H^+ at correspondingly lower D_2 mole fractions ($X_{D_2} \approx 0.12$ and 0.18).

The differences between experimental data at 71(6) K and model predictions at 80 K suggest an appreciable temperature dependence to the rates. To appreciate why, it is helpful to note that reactions only involve the H/D exchange and therefore the enthalpy change is determined solely by zero-point energy differences between reactants and products. Incorporation of D atoms via fast proton exchange re-

actions (i)–(ii), (iv), and (vi)–(vii) therefore reflect processes exoergic by $\approx$100–240 cm^{-1}, as summarized in Table III using zero-point energies for the isotopomer ions[47] and H_2, HD, and D_2 reagent.[48] Though small, these exoergicities are significant with respect to $k_B T_{rot} \approx 50\ cm^{-1}$ in the discharge expansion, which by detailed balance preferentially shifts the system toward higher steady state concentrations of both deuterated ion species at lower D_2 mole fractions.

In order to briefly explore this temperature dependence, we offer a very simple attempt to model the experimental data at 71(6) K based on the following: (1) all *exothermic* ion–molecule reaction rates (k_1, k_2, k_4, k_6, k_7) are assumed to be temperature insensitive and maintained at the 80 K values; (2) the reverse rate constants k_{-1} and k_{-7} are determined from detailed balance considerations, which for strongly endothermic reactions ($\Delta H/k_B T \approx 4.7$) yield negligibly small values at these temperatures; (3) the rate constant for reaction (v) is taken as $k_5 = 2.0 \times 10^{-10}\ cm^3\ s^{-1}$ from detailed calculations by Herbst *et al.*;[49] and (4) rate constants for the remaining two mildly endothermic reactions (k_3 and k_8) are adjusted in a least-squares process to fit the experimental data. The best fits are reported as solid lines in Fig. 8, with the inferred rate constants summarized in Table III. Given the level of approximation involved in such a steady state kinetic analysis, the agreement between experiment and simulation should be regarded as quite satisfactory.

Though such a steady state population analysis is necessarily approximate, the least-squares fits nevertheless provide some information about low temperature ion–molecule reaction rates. Based on assumptions described above, the rate coefficients for k_3 and k_8 are estimated to be $\approx$5.7 and 2.9 $\times 10^{-10}\ cm^3\ s^{-1}$. It is worth noting that both these values are approximately twofold lower than VT–SIFT experimental values,[46] which would be consistent with temperatures significantly higher than 80 K in VT–SIFT experiment. Indeed, this possibility was in fact suggested by Giles *et al.*,[46] and provides further incentive for improved rate measurements in this temperature range for these important astrophysical processes. In any event, estimates from the present work indicate that these rates could be substantially lower than previously reported.[46]

As a final topic, we briefly address the kinetic origin of the experimentally observed *ortho* versus *para* ratios in the H_2D^+ and D_2H^+ ions. This is closely related to the very interesting question of *symmetry selection rules* in chemical reactions, as investigated theoretically by Quack.[50] Indeed, the existence of such selection rules has been observed experimentally only in a few cases, most recently by Uy *et al.*[51,52] for reaction (1) and reactive collisions of H_3^+ with H_2. In these previous experiments, ratios of ortho- and para-H_3^+ spectral lines were measured in normal and para-H_2 discharges; the nonstatistical results clearly supported the existence of a ''spin memory'' for this simplest of proton exchange reactions. The slit discharge provides an opportunity to explore such spin selection rules in ion–molecule reactions under much lower temperature conditions. As shown in Fig. 2, the combination of direct absorption measurements and theoretical line strength predictions permits *absolute* populations of selected ortho and para quantum states of H_2D^+ and D_2H^+ in the slit jet to be determined. Based on (1) the experimental ortho/para ratios for these lowest states and (2) a fitted Boltzmann rotational distribution at 71(6) K, the population ratios summed over all *ortho:para* states are found to be 4.3(6): 1 and for 2.1(3):1 for H_2D^+ and D_2H^+, respectively. It is worth noting that these ortho/para population ratios are obtained from several different rotational states on the same vibrational transition, and thus should be insensitive to any error in the dipole moment surface.

The kinetic argument for rationalizing *ortho:para* ratios is most simply stated for D_2H^+. The only pathways that produce the D_2H^+ ion in the kinetic scheme developed in Sec. VI are from reactions (i), (vi), or (viii). Furthermore, it follows from the steady state ion–molecule reaction model discussed above that the total ion concentration consists of about 40% H_3^+, 35% D_2H^+, 20% H_2D^+, and 5% D_3^+ ion under an optimum $X_{D_2} \approx 0.20$. Together with the reaction rate coefficients listed in Table III, this suggests that the major pathways for total D_2H^+ ion production are (i), proton transfer between H_3^+ and D_2 (69%) and (vi), $H_2D^+ + D_2 \rightarrow D_2H^+ + HD$ (22%). In this discussion, it is important to appreciate that *steady state* rather than *equilibrium* conditions are maintained. Thus any of the several removal processes for D_2H^+ to yield (possibly) nonequilibrium ortho/para H_2 or D_2 products contribute negligibly to the overall concentrations of the n-H_2 and n-D_2 reagents. Considering spin conservation rules,[50] proton transfer can only yield ortho-D_2H^+ from ortho-D_2, with an equivalent result for para states. Consequently, the distribution of D_2H^+ states from reaction (i) should simply reflect the n-D_2 reagent, i.e., in a 2:1 *ortho:para* ratio.

Similarly, formation of D_2H^+ by reaction (vi) $H_2D^+ + D_2 \rightarrow D_2H^+ + HD$ can proceed via two mechanisms: (1) direct proton (H^+) transfer or (2) H/D exchange process between the ion and the neutral molecule. Since both pathways involve exchange of a single proton or deuteron, production of D_2H^+ ions via either process will again mirror the 2:1 *ortho:para* ratio of the n-D_2 reagent, by the same arguments presented above. Thus the dominant processes contributing to formation of D_2H^+ ion predict a 2:1 *ortho:para*, in good agreement with the 2.1(3):1 experimental value. However, this is nearly the same result anticipated for complete spin thermalization of the D_2H^+ ions, which at 71(6) K would be 2.03(2):1. Thus, the present experiment cannot unambiguously distinguish between spin thermalization or spin conservation as the predominant mechanism, though this could be readily addressed in future studies either with nonthermal (e.g., pure ortho) samples of D_2 reagent or at lower rotational temperatures.

The 4.3(6):1 *ortho:para* ratio for H_2D^+ proves more challenging to interpret. This is complicated by lower reaction exothermicities for formation of the less deuterated ion, which via detailed balance at these low experimental temperatures can significantly influence populations of various product spin states. At the optimum D_2 mole fraction ($X_{D_2} \approx 0.10$), the rate coefficients in Table III indicate two important channels for H_2D^+ production, namely $\approx$74% from reaction (iii), $D_2H^+ + H_2 \rightarrow H_2D^+ + HD$, and $\approx$26% from reac-

tion (ii), $H_3^+ + D_2 \rightarrow H_2D^+ + HD$. The former and dominant production pathway for H_2D^+ can again proceed via two mechanisms, however, both the direct deuteron (D^+) transfer and H/D exchange process should yield the same 3:1 *ortho:para* ratio with n-H_2 reagent. The second production channel for H_2D^+ ions is via H/D exchange of H_3^+ with D_2. This process is isomorphic to dissociation of $H_3^+ \rightarrow H_2^+ + H$, the spin selection rules for which have been previously derived:[50] ortho-H_3^+ yields 100% ortho-H_2^+, whereas para-H_3^+ yields 50% ortho-H_2^+ and 50% para-H_2^+. The H_3^+ is initially formed by $H_2^+ + H_2$ reactions, which for n-H_2 (i.e., 3:1 *ortho:para* ratio) has been established by Uy *et al.*[51] to generate H_3^+ in a 1:1 *ortho:para* ratio. By spin conservation with n-D_2 reagent, one then also predicts an *ortho:para* ratio of 3:1 for H_2D^+, which is again comparable to but significantly smaller than the experimentally observed H_2D^+ *ortho:para* ratio of 4.3(6). It is worth noting that since the ground state of H_2D^+ is para, spin thermalization at any finite temperature only *decreases* this ratio$\leqslant$3:1. For example, one predicts 2.30(15):1 for H_2D^+ equilibrated at 71(6) K.

Thus, the model predicts a maximum ortho/para ratio in H_2D^+ of 3:1, as opposed to the experimentally determined value of 4.3(6). This is likely due to differential exothermicities of ortho versus para reactions, which can become increasingly important at these low temperatures. By the way of example, consider reaction (iii), $H_2D^+ + H_2 \rightarrow H_2D^+ + HD$, i.e., the dominant (74%) reaction channel for producing H_2D^+. Since the lowest ortho ($J=1$) and para ($J=0$) states in H_2 differ by 118 cm^{-1}, while the lowest ortho (1_{11}) and para (0_{00}) levels in H_2D^+ differ by only 60 cm^{-1}, the endothermicity for producing o-H_2D^+ (1_{11}) is 58 cm^{-1} smaller than for p-H_2D^+ (0_{00}). This can lead to extreme enhancement of H_2D^+ ion in ortho (1_{11}) state at temperatures corresponding to $k_BT \approx 50\ cm^{-1}$. Detailed energetics for the higher states can be worked out with qualitatively similar results predicting preferential formation of ortho versus para H_2D^+. This may be of some relevance to the recent interstellar observation of ortho H_2D^+ ($1_{10} \rightarrow 1_{11}$) transitions via submillimeter emission methods.[22] In any event, the dramatic role of detailed energetics on the reaction rate coefficients has been clearly demonstrated by Gerlich,[53] who has measured rate coefficients at 10 K almost 2 orders of magnitude larger for $H_2D^+ + H_2 \rightarrow H_3^+ + HD$ using n-H_2 versus p-H_2.

VII. CONCLUSIONS

High-resolution overtone ($2\nu_2$ and $2\nu_3$) and combination band ($\nu_2+\nu_3$) spectra have been measured for jet-cooled D_2H^+ and H_2D^+ molecular ions in a slit supersonic discharge. Variational calculations have been performed using state-of-the-art relativisically corrected potential surfaces[39] for H_3^+ (and isotopomers) modified to accurately account for non-Born–Oppenheimer effects[30] due to finite coupling between nuclear and electronic motions. These first principles predictions for rovibrational term values in D_2H^+ and H_2D^+ permit detailed comparison with high-resolution experiment. The combination of these two data sets has facilitated an accurate test of non-Born–Oppenheimer dynamics, which reveals remarkably good agreement with experiment. In all transitions observed, predictions at a nearly spectroscopic level of accuracy are achieved, with systematic deviations as a function of vibration and isotopomer asymmetry providing directions for further refinement of non-Born–Oppenheimer models. Spectroscopic analysis of these data also elucidate the important role of Coriolis coupled rovibrational state mixing in both H_2D^+ and D_2H^+, which has been identified and results in a zero order rotational assignment of the high-resolution spectra. The concentrations of H_2D^+ and D_2H^+ ions in the slit jet discharge expansion have been investigated as a function of D_2/H_2 ratio in the stagnation region, and which can be quite successfully described by simple steady state kinetic analysis. Finally, steady state *ortho:para* ratios in the H_2D^+ and D_2H^+ molecular ions have been investigated, which are consistent with statistical models for spin conservation in chemical reactions, but also clearly reveal the significant influence at these low temperatures of ortho/para dependent state-to-state energetics.

ACKNOWLEDGMENTS

This work has been made possible by grants from the National Science Foundation with additional support for development of pulsed slit discharge sources from the Air Force Office of Scientific Research. Additional funding for theoretical work has been provided by the UK Engineering and Physical Sciences Research Council and the Russian Fund for Fundamental Studies. J.T. would like to express his thanks to JILA for Visiting Fellowship support at the start of this project. The authors also wish to thank Professor Dieter Gerlich for providing information on low rate coefficients for ion molecule reactions prior to publication.

[1] B. J. McCall and T. Oka, Science **287**, 1941 (2000).
[2] P. Drossart, J.-P. Maillard, J. Caldwell, S. J. Kim, J. K. G. Watson, W. A. Majewski, J. Tennyson, S. Miller, S. K. Atreya, J. T. Clarke, J. J. H. Waite, and R. Wagener, Nature (London) **340**, 539 (1989).
[3] T. R. Geballe, M. F. Jagod, and T. Oka, Astrophys. J. Lett. **408**, L109 (1993).
[4] T. Oka and T. R. Geballe, Astrophys. J. Lett. **351**, L53 (1990).
[5] T. R. Geballe and T. Oka, Nature (London) **384**, 334 (1996).
[6] B. J. McCall, K. H. Hinkle, T. R. Geballe, and T. Oka, Faraday Discuss. **109**, 267 (1998).
[7] B. J. McCall, T. R. Geballe, K. H. Hinkle, and T. Oka, Astrophys. J. **522**, 338 (1999).
[8] T. R. Geballe, B. J. McCall, K. H. Hinkle, and T. Oka, Astrophys. J. **510**, 251 (1999).
[9] B. J. McCall, T. R. Geballe, K. H. Hinkle, and T. Oka, Science **279**, 1910 (1998).
[10] T. Oka, Rev. Mod. Phys. **64**, 1141 (1992).
[11] S. Miller and J. Tennyson, Chem. Soc. Rev. **21**, 281 (1992).
[12] A. Dalgarno, Adv. At., Mol., Opt. Phys. **58**, 57 (1994).
[13] I. R. McNab, Adv. Chem. Phys. **89**, 1 (1994).
[14] S. Miller, H. A. Lam, and J. Tennyson, Can. J. Phys. **72**, 760 (1994).
[15] J. Tennyson, Rep. Prog. Phys. **58**, 421 (1995).
[16] T. Oka, Phys. Rev. Lett. **45**, 531 (1980).
[17] J. K. G. Watson, S. C. Foster, A. R. W. McKellar, P. Bernarth, T. Amano, F. S. Pan, M. W. Crofton, R. S. Altman, and T. Oka, Can. J. Phys. **62**, 1875 (1984).
[18] D. Uy, C. M. Gabrys, M.-F. Jagod, and T. Oka, J. Chem. Phys. **100**, 6267 (1994).
[19] S. S. Lee, B. F. Ventrudo, D. T. Cassidy, T. Oka, S. Miller, and J. Tennyson, J. Mol. Spectrosc. **145**, 222 (1991).

[20] L.-W. Xu, C. Gabrys, and T. Oka, J. Chem. Phys. **93**, 6210 (1990).
[21] M. G. Bawendi, B. D. Rehfuss, and T. Oka, J. Chem. Phys. **93**, 6200 (1990).
[22] R. Stark, F. F. S. van der Tak, and E. F. van Dishoeck, Astrophys. J. Lett. **521**, L67 (1999).
[23] T. Amano and J. K. G. Watson, J. Chem. Phys. **81**, 2869 (1984).
[24] S. C. Foster, A. R. W. McKellar, I. R. Peterkin, J. K. G. Watson, F. S. Pan, M. W. Crofton, R. S. Altman, and T. Oka, J. Chem. Phys. **84**, 91 (1986).
[25] S. C. Foster, A. R. W. McKellar, and J. K. G. Watson, J. Chem. Phys. **85**, 664 (1986).
[26] O. L. Polyansky and A. R. W. McKellar, J. Chem. Phys. **92**, 4039 (1990).
[27] J. Tennyson and O. L. Polyansky, Phys. Rev. A **50**, 314 (1994).
[28] B. M. Dinelli, C. R. L. Sueur, J. Tennyson, and R. D. Amos, Chem. Phys. Lett. **232**, 295 (1995).
[29] B. M. Dinelli, O. L. Polyansky, and J. Tennyson, J. Chem. Phys. **103**, 10433 (1995).
[30] O. L. Polyansky and J. Tennyson, J. Chem. Phys. **110**, 5056 (1999).
[31] D. T. Anderson, S. Davis, T. S. Zwier, and D. J. Nesbitt, Chem. Phys. Lett. **258**, 207 (1996).
[32] S. Davis, D. T. Anderson, G. Duxbury, and D. J. Nesbitt, J. Chem. Phys. **107**, 5661 (1997).
[33] S. Davis, M. Fárník, D. Uy, and D. J. Nesbitt, Chem. Phys. Lett. **344**, 23 (2001).
[34] A. S. Pine, J. Opt. Soc. Am. **64**, 1683 (1974).
[35] T. Amano, J. Chem. Phys. **79**, 3595 (1983).
[36] E. Riedle, S. H. Ashworth, J. T. Farrell, and D. J. Nesbitt, Rev. Sci. Instrum. **65**, 42 (1994).
[37] R. B. Leblanc, J. B. White, and P. F. Bernath, J. Mol. Spectrosc. **164**, 574 (1994).
[38] R. Röhse, W. Kutzelnigg, R. Jaquet, and W. Klopper, J. Chem. Phys. **101**, 2231 (1994).
[39] W. Cencek, J. Rychlewski, R. Jaquet, and W. Kutzelnigg, J. Chem. Phys. **108**, 2831 (1998).
[40] P. R. Bunker and R. E. Moss, Mol. Phys. **33**, 417 (1977).
[41] P. R. Bunker, C. J. McLarnon, and R. E. Moss, Mol. Phys. **33**, 425 (1977).
[42] R. E. Moss, Mol. Phys. **89**, 195 (1996).
[43] R. E. Moss and D. Jopling, Chem. Phys. Lett. **260**, 377 (1996).
[44] J. Tennyson *et al.* (unpublished).
[45] R. H. Judge and D. J. Clouthier, Comput. Phys. Commun. **135**, 293 (2001).
[46] K. Giles, N. G. Adams, and D. Smith, J. Phys. Chem. **96**, 7645 (1992).
[47] G. D. Carney, Chem. Phys. **54**, 103 (1980).
[48] K. P. Huber and G. Herzberg, *Molecular Spectra and Molecular Structure. IV. Constants of Diatomic Molecules* (Van Nostrand, New York, 1979).
[49] E. Herbst, Astron. Astrophys. **111**, 76 (1982).
[50] M. Quack, Mol. Phys. **34**, 477 (1977).
[51] D. Uy, M. Cordonnier, and T. Oka, Phys. Rev. Lett. **78**, 3844 (1997).
[52] M. Cordonnier, D. Uy, R. M. Dickson, K. E. Kerr, Y. Zhang, and T. Oka, Chem. Phys. **113**, 3181 (2000).
[53] D. Gerlich (private communication).